RSC Advances

PAPER

View Article Online
View Journal | View Issue

Cite this: *RSC Adv.*, 2022, **12**, 33598

One-step thermal polymerization synthesis of nitrogen-rich g-C_3N_4 nanosheets enhances photocatalytic redox activity†

Leyu Peng, [a] Jiaxi Liu,[ab] Ziyuan Li,[a] Yifan Jing,[a] Yongjin Zou,[a] Hailiang Chu, [a] Fen Xu, [a] Lixian Sun *[ab] and Pengru Huang *[a]

Graphitic carbon nitride (g-C_3N_4) has attracted enormous attention as a visible-light-responsive carbon-based semiconductor photocatalyst. However, fast charge recombination seriously limits its application. Therefore, it is urgent to modify the electronic structure of g-C_3N_4 to obtain excellent photocatalytic activity. Herein, we reported a one-step thermal polymerization synthesis of nitrogen-rich g-C_3N_4 nanosheets. Benefiting from the N self-doping and the ultrathin structure, the optimal CN-70 exhibits its excellent performance. A 6.7 times increased degradation rate of rhodamine B (K = 0.06274 min^{-1}), furthermore, the hydrogen evolution efficiency also reached 2326.24 μmol h^{-1} g^{-1} (λ > 420 nm). Based on a series of characterizations and DFT calculations, we demonstrated that the N self-doping g-C_3N_4 can significantly introduce midgap states between the valence band and conduction band, which is more conducive to the efficient separation of photogenerated carriers. Our work provides a facile and efficient method for self-atom doping into g-C_3N_4, providing a new pathway for efficient photocatalysts.

Received 17th September 2022
Accepted 15th November 2022

DOI: 10.1039/d2ra05867g

rsc.li/rsc-advances

Introduction

Since the industrial revolution, the ecological imbalance and resource depletion have seriously restricted the sustainable development of society.[1] Semiconductor photocatalytic technology has been deemed an effective strategy to solve environmental and energy shortage problems.[2–5] Graphitic carbon nitride (g-C_3N_4), an organic polymer composed of two nonmetals (C and N), has attracted much observation owing to its simple preparation method, excellent electronic structure, and stable physicochemical properties.[6–9] The photocatalytic efficiency of g-C_3N_4 is mainly determined by the generation, separation, migration, and conversion of photogenerated charges on the semiconductor surface and interface. However, due to the limitations of inefficient utilization of visible light, the high recombination rate of photo-induced electron–hole pairs, and low surface area, the bulk g-C_3N_4 often has inadequate photocatalytic efficiency.[10–12] To address the above mentioned problems, various modification methods, such as doping foreign elements, morphology design, constructing a heterojunction with g-C_3N_4-based, and engineering defects with vacancies, have emerged to enhance the photocatalytic activity.[13–18]

Doping heteroatoms, such as B, S, Cl, and P elements in g-C_3N_4, are considered to be an easy and effective way to enhance photocatalytic activity. However, this approach still has drawbacks, the introduction of heteroatoms may be a charge recombination center to affect the migration path of photo-generated charges, which can further lead to thermal instability.[19] For g-C_3N_4, N self-doping can not only tune the electronic structure but also avoid the introduction of foreign atoms, thereby enhancing photocatalytic activity. Moreover, the modification of the g-C_3N_4 structure has been also considered one of the effective strategies to improve catalytic efficiency. Currently, there are two approaches (top-down and bottom-up) for creating ultrathin 2D g-C_3N_4 structures. However, the top-down strategies typically involve strong acid treatment, and ultrasonication treatment, which generally cause multi-steps, longer, and energy-consuming.[20,21] Besides, the ultrathin 2D g-C_3N_4 structure can also be directly obtained by bottom-up strategies. For instance, Wu *et al.* prepared 2D ultrathin g-C_3N_4 nanosheets by using ammonium chloride as the gas template and dicyandiamide as the precursor.[22] Fang *et al.* used the Ni-foam as the template and catalyst to synthesize 2D g-C_3N_4 nanosheets.[23] But most of the reported preparation of 2D g-C_3N_4 nanosheets requires additional gas templates, which can pollute the environment. Hence, it is necessary to develop a simple and "green" routine for ultrathin

[a]*School of Material Science and Engineering, Guilin University of Electronic Technology, Guangxi Key Laboratory of Information Materials, Guangxi Collaborative Innovation Center of Structure and Property for New Energy and Materials, Guilin 541004, China. E-mail: pengruhuang@guet.edu.cn*

[b]*School of Mechanical & Electrical Engineering, Guilin University of Electronic Technology, Guilin 541004, China. E-mail: sunlx@guet.edu.cn*

† Electronic supplementary information (ESI) available. See DOI: https://doi.org/10.1039/d2ra05867g

2D g-C_3N_4 nanosheets to trigger an excellent photocatalytic performance.

Herein, we creatively report a one-step thermal polymerization synthesis of nitrogen-rich two-dimensional g-C_3N_4 nanosheets. Methanol molecules as an additive can boost the production of more gaseous by decomposing urea during thermal polymerization, which can be obtained in ultrathin 2D porous g-C_3N_4 nanosheets under the gas-shocking exfoliation. And the methanol would undergo an ammoniation reaction at 370–420 °C to generate nitrogen-containing compounds and water molecules. The nitrogen-containing compounds can provide an N source as a dopant during the heat treatment process. On the base of the investigations of structure and photoelectrical measurement, we showed that the enlarged specific surface area and efficient charge transport are more conducive to the progression of photocatalytic reactions. Density functional theory calculations demonstrated that the N self-doping g-C_3N_4 can significantly introduce midgap states to facilitate the effective separation of electron–hole pairs. Benefiting from these advantages, the CN-70 showed excellent photocatalytic activity in both degradation of rhodamine B and water splitting.

Experimental section

Chemical reagent

Urea, methanol, rhodamine B (RhB), triethanolamine (TEOA), isopropyl alcohol (IPA), ethylenediamine tetra acetic acid disodium salt (EDTA-2Na), and benzoquinone (BQ) were of analytical grade purchased commercially and used without further purification.

Synthesis of CN and CN-*X* (*X* = 30, 50, 70, 90)

In a typical procedure, 6.372 g of urea is into an agate mortar and ground into a uniform powder for about 30 minutes and the uniform powder is dissolved into 70 ml methanol to form a clear transparent solution. To achieve a mixed thoroughly solution, the urea-methanol mixture solution was transferred into a water bath at 50 °C, accompanied by continuously stirring. After 30 minutes, the homogeneous solution was poured into a 100 ml covered crucible and placed in a muffle furnace, then heated from room temperature to 550 °C at 2.5 °C min^{-1} and kept this temperature for 4 h. After natural cooling later, the light pale yellow powder was fully washed to remove impurities and dried, which was abbreviated CN-70. The CN-*X* (*X* = 30, 50, 90) samples were synthesized as same as CN-70, except that the amount of methanol used in the step was different (30 ml, 50 ml, and 90 ml, respectively). In addition, the bulk g-C_3N_4 samples were prepared according to the reported literature as a comparison. 6.372 g urea uniform powder was directly thermal polymerization under the same condition, named CN.

The detail characterizations, photocatalytic activity measurements and DFT calculation methods are exhibited in the ESI.†

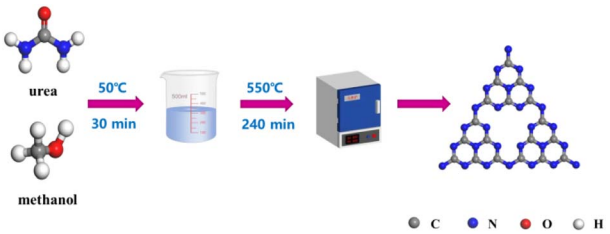

Scheme 1 The synthesis procedure of CN-*X*.

Results and discussion

The one-step thermal copolymerization strategy is shown in Scheme 1. In this procedure, CN-*X* was obtained by calcining a mixed solution of urea and methanol. Methanol and urea would undergo an ammoniation reaction at 370–420 °C to generate nitrogen-containing compounds and water molecules. Urea would release massive gaseous (NH_3, H_2O, and CO_2) under heat treatment. The nitrogen-containing compounds can provide N atoms as deposition elements. These gases could promote the formation of 2D porous morphology. At last, ultrathin 2D porous nitrogen-rich CN-*X* was obtained.

The X-ray powder diffraction (XRD) patterns were used to analyze the crystal structure.[24] Fig. 1a showed that all the samples show similar peaks at 2θ = 13.1° or 27.3°, corresponding to the (100) plane and (002) plane of g-C_3N_4 sheets, respectively.[25] For CN-70, the peak intensities at 27.3° are significantly decreased, which verified that the bulk g-C_3N_4 has been successfully exfoliated into nanosheets (Fig. S1a†).[26] Fig. 1b showed the chemical structures by Fourier transform infrared (FTIR) spectroscopy, the 810 cm^{-1} peak represents the out-of-plane bending mode of heptazine rings, and the typical 1200–1700 cm^{-1} peak can be assigned to the CN heterocycles, and the broad peak between 3000 and 3400 cm^{-1} is related to the N–H group and the O–H group.[26] Fig. S1b† showed that the FTIR peak of the CN-*X* samples is weaker than that of CN, this phenomenon is attributed to the possible structural disorder of CN-*X* samples.[27] XRD and FTIR results showed that the crystal structure of CN-*X* was preserved.

Fig. S2† shows the SEM and TEM images of the CN and CN-70 samples. The CN exhibited typical layered platelet-like structure.[28] In the meanwhile, it is very easy to notice that the CN-70 obtained more in-plane porous structure and more curly edges compared with CN. The TEM image of CN-70 is like a translucent silk structure that looks very thin.[24] The above-mentioned morphological changes can be attributed to the impact of the gas-shocking exfoliation during the calcination process. The in-plane pores on the surface of CN-70 can not only effectively increase the catalytic active sites and improve mass transfer, but also hinder the re-aggregation of nanosheets during the photocatalytic process,[29] which is beneficial to improve the catalytic activity and stability. In addition, the structure of CN-70 motivated us to examine its pore structure and specific surface area. Fig. 1c shows that both CN and CN-70 samples have type-IV isotherms, which represent a mesoporous

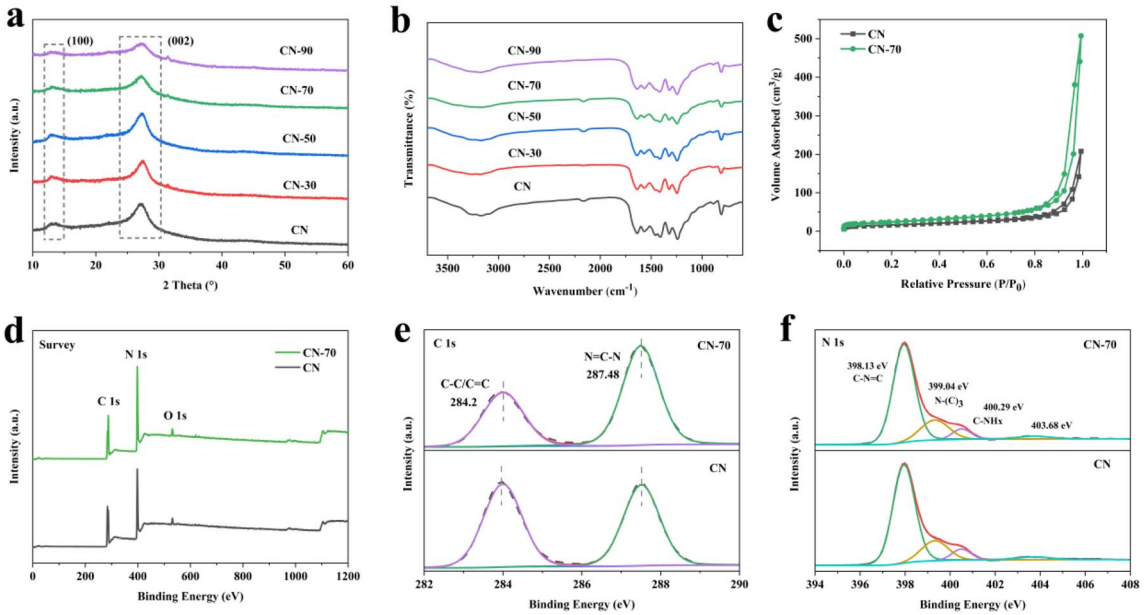

Fig. 1 (a) The XRD patterns, (b) the FTIR spectra of CN, CN-*X* (*X* = 30, 50, 70, 90), (c) N_2 adsorption/desorption isotherms, (d) XPS survey spectra, and (e and f) the high-resolution XPS spectra of C 1s, N 1s, for CN and CN-70.

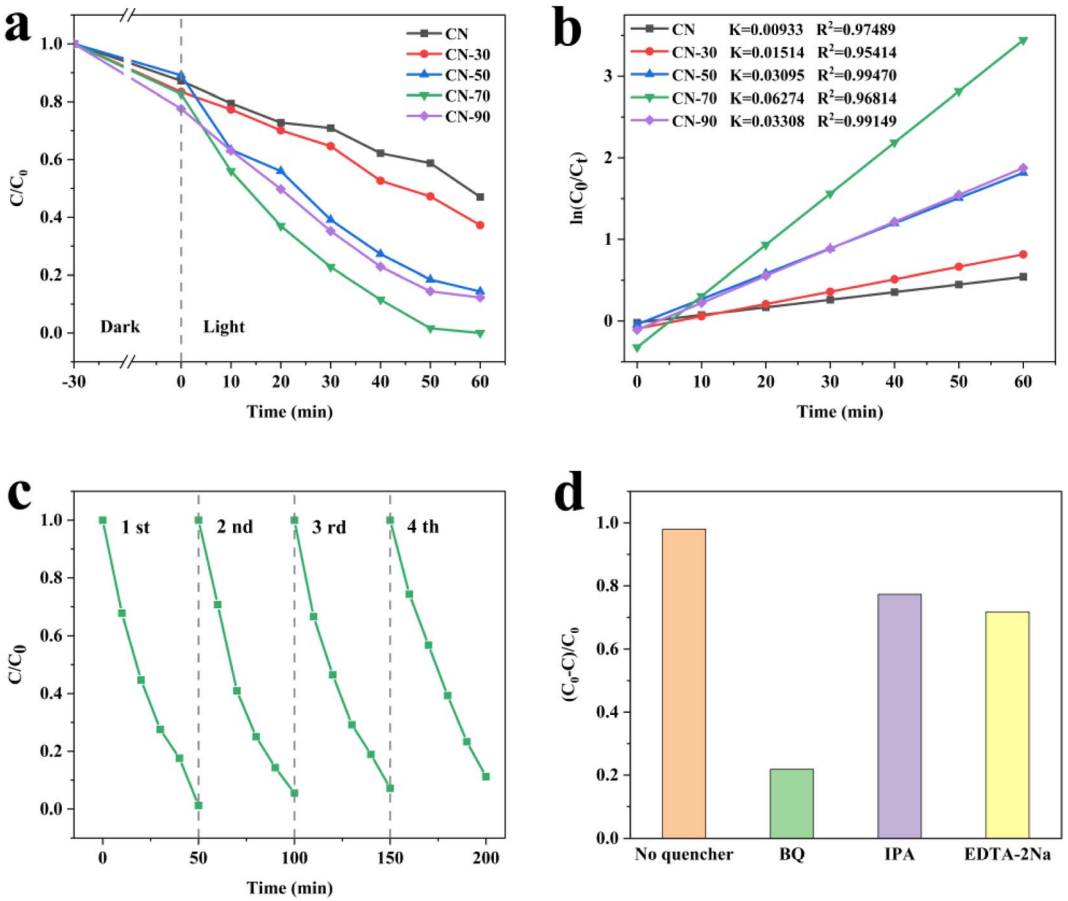

Fig. 2 (a) Photocatalytic degradation curves, (b) first-order kinetics curves of CN and CN-*X*, (c) cycle experiments of the RhB degradation, and (d) photocatalytic performance of in the presence of different trapping agents of CN-70.

structure.[30] And CN-70 specific surface was calculated to reach 86.5 $m^2\ g^{-1}$, showing a higher than CN (Table S1†). The data show that CN-70 can provide more surface active sites, which is more conducive to the photocatalytic process.

To investigate the elemental compositions and chemical states of g-C_3N_4, XPS analysis was performed. The XPS survey spectra show that C, N, and O elements were presented in CN and CN-70. The spectra of C 1s centered at 284.2 eV and 287.48 eV, which can be attributed to C–C/C=C and N=C–N, respectively (Fig. 1e).[31] The spectra of N 1s can be fitted with four main peaks, which are attributed to the C–N=C at 398.13 eV, N_3C-low binding energy at 399.3 eV and N_3C-high binding energy at 400.29 eV, and π-excitation, $-NH_2$ groups or N–N bonds at 403.68 eV, respectively.[32–35] By analyzing the peak area (Tables S2 and S3†), CN-70 showed a reduced C content and an increased N content, which further proved that the CN-70 surface is nitrogen-enriched after methanol modification. This conclusion can be attributed to the fact that some carbon atoms were replaced by nitrogen atoms in g-C_3N_4 during the heat-treatment.

The photo-degradation activities of the samples were evaluated by RhB degradation under visible-light irradiation. Fig. 2a shows all of the samples photocatalytic degradation curves. It can be seen that all the CN-*X* samples show strengthened photo-degradation efficiency activity. Among the different proportions of catalysts, CN-70 exhibits excellent degradation efficiency. By fitting the first-order kinetics, as shown in Fig. 2b, the CN-70 can reach 0.06274 min^{-1}, which is about 6.72 times upper than that of CN (0.00933 min^{-1}). In addition, the RhB removal ratio of CN-70 is supper than most of the g-C_3N_4-based photocatalysts reported in the literature (Table S5†) to investigate the stability of the photocatalyst, we performed four cycle experiments on CN-70, as shown in Fig. 2c, the CN-70 still maintains a great activity. The slight decrease in photocatalytic activity contributes to the loss of the photocatalyst during the washing process after each run. Some sacrificial agents are put into photocatalytic reactions to study the main active species in RhB photo-degradation. The IPA, EDTA-2Na and BQ were used to trap $^{\bullet}OH$, h^+ and $^{\bullet}O_2^-$, respectively. The degradation rate of RhB significantly decreased when BQ was added (Fig. 2d), this phenomenon indicates that $^{\bullet}O_2^-$ was the main active species of CN-70 in the photocatalytic degradation of RhB. Moreover, the addition of EDTA-2Na and IPA also inhibited the degradation, indicating that the h^+ and $^{\bullet}OH$ also played an auxiliary role.

Furthermore, to study the photocatalytic reduction activity, we tested the hydrogen production under visible light irradiation. It can be observed that the H_2 production amount for the CN-*X* samples increases, achieving a maximum for CN-70 (Fig. S4†). The calculated H_2 evolution rate of CN-70 reaches 2326.24 μmol $h^{-1}\ g^{-1}$, which is more excellent than most of the g-C_3N_4-based photocatalysts reported by literature (Table S6†). CN-70 exhibits in excellent activities in both photodegradation RhB and H_2 evolution, which may indicate that 70 ml is a relatively good proportion.

After modified urea with methanol, the absorption edges of CN-*X* showed an obvious red shift phenomenon, which could broaden its absorption range of visible light (Fig. S3†). As shown in Fig. 3a. Based on the Kubelka–Munk method, the bandgaps were estimated to be 2.84 eV and 2.68 eV of CN and CN-70, respectively.[36,37] The CN-70 possessed a narrower bandgap than CN, allowing increased utilization of the solar spectrum and the potential to generate more photo-generated electron–hole pairs under visible light. The valence band (VB) XPS measurements were carried out to estimate energy levels. The VB spectra of CN and CN-70 were estimated to be 1.67 and 1.50 eV (*vs.* NHE), respectively (Fig. 3b).

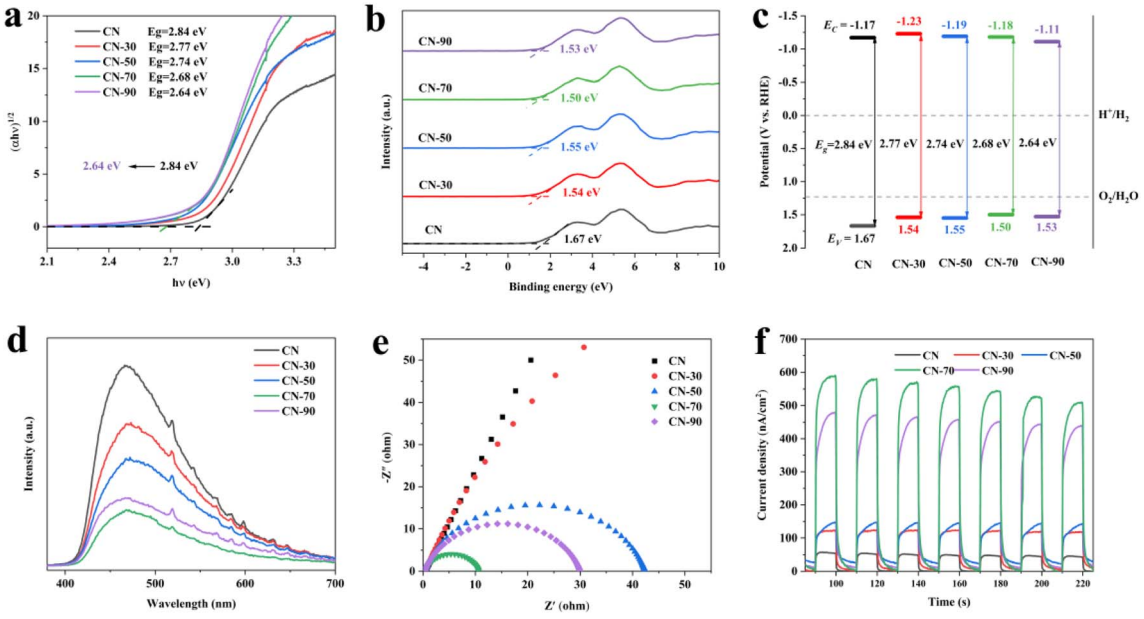

Fig. 3 (a) Bandgaps, (b) VB-XPS measurements, (c) band structure diagrams, (d) PL, (e) EIS, and (f) TPR changes of CN and CN-*X*.

Through the bandgaps and the VB-XPS, the CB of CN and CN-70 were also estimated to be −1.17 and −1.18 eV respectively.[38] Combined with the above data analysis, the narrower bandgap may originate from VB potentials of the CN-*X* becoming more positive, which can conducive to the photocatalytic redox reaction. However, considering ˙OH also played an auxiliary role in RhB degradation process, but the ˙OH could not be generated directly because the VB potential of the sample falls short of the potential of OH^-/˙OH (1.99 V), so we tested the ESR spectra of ˙OH for CN-70 sample. As shown in Fig. S8,† obviously, no signal peaks of DMPO–˙OH was detected under dark conditions, but obvious signal peaks of DMPO–˙OH was detected under light conditions. In the meanwhile, DMPO–˙OOH was also suspected detect in this process, this phenomenon can be attributed to $\cdot O_2^-$ can accept an H^+ to form ˙OOH.[39] Both DMPO–˙OOH and DMPO–˙OH lead to superposition of the spectra. The experimental result further proves that ˙OH is generated in the photocatalytic system.[40]

The photoluminescence (PL) and time-resolved transient PL decay spectra were carried out to get a deeper understanding of charge transport efficiency.[41] All the CN-*X* samples show a lower peak activity (Fig. 3d). Among them, the CN-70 sample exhibits the lowest PL intensity, this phenomenon can be attributed to the electron–hole pairs can be effectively separated and results in substantial PL quenching for CN-*X* samples. Besides, as shown in Table S4,† CN-70 exhibits a long PL lifetime with an average lifetime of about 6.58 ns, which is 2.5 times that of CN (2.64 ns), further indicating the improved separation efficiency of photo-generated electron–hole pairs.[42] Moreover, electrochemical impedance spectra (EIS) were used to research the resistivity of the samples. CN-70 has the smallest arc radius compared with all samples (Fig. 3e), indicating it's smallest charge transfer resistance and efficient interfacial charge transfer. Fig. 3f shows the transient photoelectric response (TPR) test for several on–off cycles of intermittent irradiation, we found that CN-70 has the strongest current density, which is about 11 times that of CN. The enhanced photoelectronic performance of CN-70 can be attributed to the abundant in-plane hole structure, which greatly facilitates the separation and migration of photo-generated carriers. Combined with the photo-electronic characterizations, it can be inferred that the modification of methanol can promote the mass transfer and separation of photo-generated carriers, and its performance is the best when the methanol addition amount is 70 ml.

Based on XPS and other characterizations, we proposed that the N self-doping in g-C_3N_4. To further understand the impact

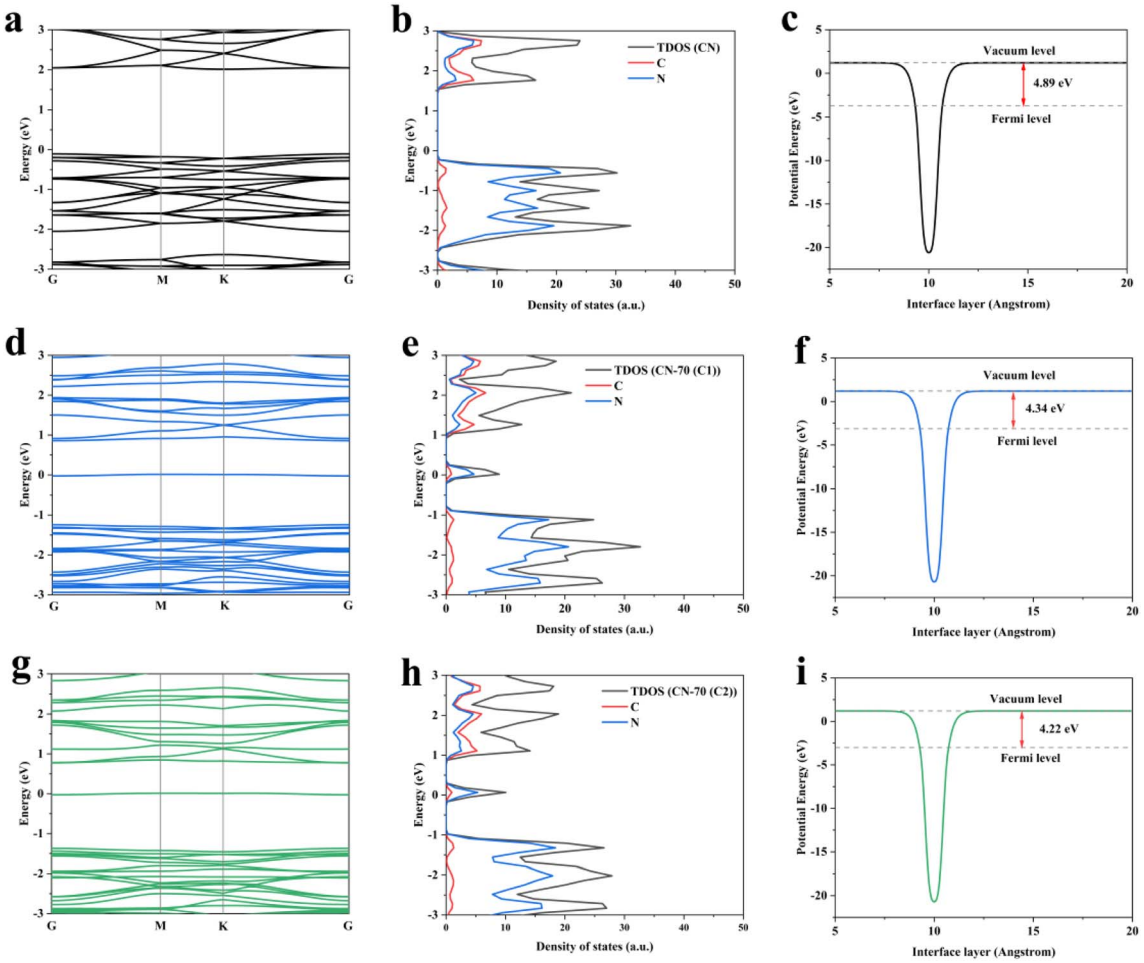

Fig. 4 (a, d and g) Electronic band structures, (b, e and h) density of states, (c, f and i) work function of CN, CN-70(C1) and CN-70(C2).

of N atom self-doping in g-C_3N_4, we used VASP based on density functional theory (DFT) calculation to further explain the enhanced photocatalytic performance (Fig. 4).[43,44] It was not difficult to find that there are two C sites at different positions in the g-C_3N_4 structure, which provide two doping possibilities for N, namely C1 and C2, respectively (Fig. S5†). By calculating the electronic structure of the CN, CN-70(C1), and CN-70(C2), we found that the N self-doping g-C_3N_4 at C1/C2 site possess similar band structures and density of states. The introduction of midgap states can reduce the migration path of the photo-generated electrons, which is in accordance with the photo-electrical measurement results. In addition, we performed the calculation of the work function. The calculation results show that the work functions of the CN-70(C1) and CN-70(C2) are both reduced, which indicates that N self-doping can promote the escape of electrons from the surface of g-C_3N_4. These results not only can cause more electrons react with O_2 generate more $^{\cdot}O_2^-$ active radical but also can participate in the H^+ reduction to generate H_2, which is helpful for the process of the photocatalytic redox reactions. Hence, the shortened charge transmission path, enhanced escape ability of electrons, and more efficient separation of electron–hole pairs also result in a redshift for visible light absorption (Fig. S6†), consistent with experimental data.

Based on the above experiment characterizations and theoretical calculations, a reasonable photocatalytic reaction can be described for this work (Fig. 5). The introduction of nitrogen self-doping shortens the bandgaps and promotes its visible-light absorption, allowing more photo-generated carriers to participate in the reaction under visible light irradiations. Moreover, the nitrogen self-doping also introduces midgap states, which not only can accept electrons from the CB of the catalyst to inhibit the recombination process of the photo-generated e^- and h^+ but also shorten the photo-generated electrons' migration path, in this process, the electrons were combined with oxygen to form $^{\cdot}O_2^-$, more h^+ were left in VB, both can oxidize organic pollutions. Meanwhile, the porous structure could enlarge the special surface area to provide more catalytically active sites. Benefiting from the above advantages, a significantly increased photocatalytic redox activity by CN-70 can be obtained.

The optimized CN-70 exhibited excellent degradation of rhodamine B rate and photocatalytic hydrogen evolution compared with the previously reported g-C_3N_4-based literature (Tables S5 and S6†). Just by controlling the amount of methanol added, we obtained highly efficient g-C_3N_4 based photocatalysts. After considering the information above, we conclude that excellent photocatalytic activity of the CN-70 is attributable to the following factors: firstly, N self-doping g-C_3N_4 can significantly introduce midgap states, which is more conducive to the efficient separation of photo-generated carriers. Secondly, the porous structure can offer more reaction sites, thereby acceleration the photochemical reactions. And the synergistic effect of the two further improves the catalytic activity.

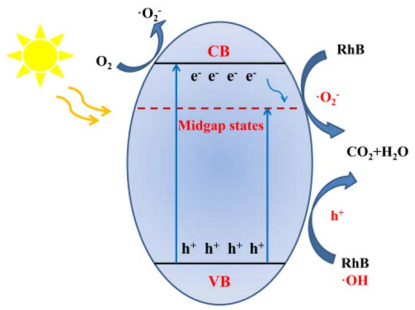

Fig. 5 The proposed reaction mechanism.

Conclusions

In summary, nitrogen-rich ultrathin porous g-C_3N_4 nanosheets had been successfully synthesized by one-step thermal copolymerization of the urea-methanol solution method. By controlling the amount of methanol added, the final CN-70 exhibited excellent photocatalytic hydrogen evolution (2326.24 μmol h^{-1} g^{-1}) and degradation of organic pollutants RhB rate (K = 0.06274 min^{-1}). Combining XPS analysis, photoelectric experiments, trapping agents experiments and DFT calculations, we found that the formation of N self-doping can not only shorten the migration path of photo-generated electrons and further accelerate the separation of carriers, but also promote the escape of electrons from the surface to further facilitate the formation of $^{\cdot}O_2^-$ radicals. Importantly, this work also provides a facile method for the large-scale production of high-quality ultrathin nitrogen-rich g-C_3N_4-based photocatalysts through a thermal copolymerization strategy.

Author contributions

Leyu Peng (first author): conceptualization, investigation, methodology, formal analysis, writing-original draft; Jiaxi Liu: investigation; Ziyuan Li: data curation; Yifan Jing: investigation; Hailiang Chu: supervision. Yongjin Zou: project administration, supervision; Fen Xu: supervision; Lixian Sun (corresponding author): financial support, resources, supervision; Pengru Huang (corresponding author): financial support, project administration, resources, writing-review & editing.

Conflicts of interest

There are no conflicts to declare.

Acknowledgements

This work was supported by the National Key Research and Development Program of China (Grant No. 2021YFB3802400), National Natural Science Foundation of China (Grant No. 52161037, U20A20237, 51871065, 51971068), the Scientific Research and Technology Development Program of Guangxi (Grant No. AD19110037, AA19182014, AD17195073, AA17202030-1), Guangxi Natural Science Foundation (Grant No. 2017JJB150085, 2019GXNSFGA245005), the Innovation Project of GUET Graduate Education, China (Grant No. 2022YCXS197), the Guangxi Bagui Scholar Foundation, Guangxi Collaborative

Innovation Center of Structure and Property for New Energy and Materials, Guangxi Advanced Functional Materials Foundation and Application Talents Small Highlands, Chinesisch-Deutsche Kooperationsgruppe (No. GZ1528), Guilin Lijiang Scholar Foundation, Science and Technology Development Project of Guilin (20210102-4, 20210216-1).

Notes and references

1 M. A. Alenizi, R. Kumar, M. Aslam, F. A. Alseroury and M. A. Barakat, *Sci. Rep.*, 2019, **9**, 12091.
2 S. A. Ansari and M. H. Cho, Simple and Large Scale, *Sci. Rep.*, 2017, **7**, 43055.
3 W. Tahir, T.-Y. Cheang, J.-H. Li, C. Ling, X.-J. Lu, I. Ullah, G. Wang and A.-W. Xu, *Catal. Sci. Technol.*, 2022, **12**, 2023–2029.
4 N. Bhandary, A. P. Singh, S. Kumar, P. P. Ingole, G. S. Thakur, A. K. Ganguli and S. Basu, *ChemSusChem*, 2016, **9**, 2816–2823.
5 M. Cao, K. Wang, I. Tudela and X. Fan, *Appl. Surf. Sci.*, 2021, **536**, 147784.
6 M. Chen, R. Bai, P. Jin, J. Li, Y. Yan, A. Peng and J. He, *J. Alloys Compd.*, 2021, **869**, 159292.
7 K. Fan, Z. Jin, H. Yang, D. Liu, H. Hu and Y. Bi, *Sci. Rep.*, 2017, **7**, 7710.
8 R. C. Pawar, S. Kang, J. H. Park, J.-h. Kim, S. Ahn and C. S. Lee, *Sci. Rep.*, 2016, **6**, 31147.
9 B. Fei, Y. Tang, X. Wang, X. Dong, J. Liang, X. Fei, L. Xu, Y. Song and F. Zhang, *Mater. Res. Bull.*, 2018, **102**, 209–217.
10 C. Feng, L. Tang, Y. Deng, J. Wang, Y. Liu, X. Ouyang, H. Yang, J. Yu and J. Wang, *Appl. Catal., B*, 2021, **281**, 119539.
11 J. Feng, D. Zhang, H. Zhou, M. Pi, X. Wang and S. Chen, *ACS Sustainable Chem. Eng.*, 2018, **6**, 6342–6349.
12 J. Fu, K. Liu, K. Jiang, H. Li, P. An, W. Li, N. Zhang, H. Li, X. Xu, H. Zhou, D. Tang, X. Wang, X. Qiu and M. Liu, *Adv. Sci.*, 2019, **6**, 1900796.
13 Y. Huang, L. Ning, Z. Feng, G. Ma, S. Yang, Y. Su, Y. Hong, H. Wang, L. Peng and J. Li, *Environ. Sci.: Nano*, 2021, **8**, 460–469.
14 W. Iqbal, B. Yang, X. Zhao, M. Rauf, M. Waqas, Y. Gong, J. Zhang and Y. Mao, *Catal. Sci. Technol.*, 2018, **8**, 4576–4599.
15 D. Jia, Y. Zhang, X. Zhang, P. Feng, L. Yang, R. Ning, H. Pan and Y. Miao, *Environ. Sci.: Nano*, 2021, **8**, 415–431.
16 H. Katsumata, Y. Tachi, T. Suzuki and S. Kaneco, *RSC Adv.*, 2014, **4**, 21405–21409.
17 Y. Li, R. Jin, Y. Xing, J. Li, S. Song, X. Liu, M. Li and R. Jin, *Adv. Energy Mater.*, 2016, **6**, 1601273.
18 W. Liu, N. Iwasa, S. Fujita, H. Koizumi, M. Yamaguchi and T. Shimada, *Appl. Surf. Sci.*, 2020, **499**, 143901.
19 Z. Mo, H. Xu, Z. Chen, X. She, Y. Song, J. Wu, P. Yan, L. Xu, Y. Lei, S. Yuan and H. Li, *Appl. Catal., B*, 2018, **225**, 154–161.
20 M. A. Mohamed, M. F. M. Zain, L. Jeffery Minggu, M. B. Kassim, N. A. Saidina Amin, W. N. W. Salleh, M. N. I. Salehmin, M. F. Md Nasir and Z. A. Mohd Hir, *Appl. Catal., B*, 2018, **236**, 265–279.
21 A. Naseri, M. Samadi, A. Pourjavadi, A. Z. Moshfegh and S. Ramakrishna, *J. Mater. Chem. A*, 2017, **5**, 23406–23433.
22 X. Lu, K. Xu, P. Chen, K. Jia, S. Liu and C. Wu, *J. Mater. Chem. A*, 2014, **2**, 18924–18928.
23 Z. Fang, Y. Hong, D. Li, B. Luo, B. Mao and W. Shi, *ACS Appl. Mater. Interfaces*, 2018, **10**, 20521–20529.
24 P.-l. Li, Y.-h. Wang, M. Shang, L.-f. Wu and X.-X. Yu, *Carbon*, 2020, **159**, 1–8.
25 P. Su, J. Zhang, K. Xiao, S. Zhao, R. Djellabi, X. Li, B. Yang and X. Zhao, *Chin. J. Catal.*, 2020, **41**, 1894–1905.
26 Q. Tay, P. Kanhere, C. F. Ng, S. Chen, S. Chakraborty, A. C. H. Huan, T. C. Sum, R. Ahuja and Z. Chen, *Chin. J. Catal.*, 2015, **27**, 4930–4933.
27 Z. Teng, N. Yang, H. Lv, S. Wang, M. Hu, C. Wang, D. Wang and G. Wang, *Chemistry*, 2019, **5**, 664–680.
28 D. Zhu and Q. Zhou, *Appl. Catal., B*, 2021, **281**, 119474.
29 Z. Li, Q. Chen, Q. Lin, Y. Chen, X. Liao, H. Yu and C. Yu, *J. Taiwan Inst. Chem. Eng.*, 2020, **114**, 249–262.
30 N. Tian, Y. Zhang, X. Li, K. Xiao, X. Du, F. Dong, G. I. N. Waterhouse, T. Zhang and H. Huang, *Nano Energy*, 2017, **38**, 72–81.
31 H. Tran Huu, M. D. N. Thi, V. P. Nguyen, L. N. Thi, T. T. T. Phan, Q. D. Hoang, H. H. Luc, S. J. Kim and V. Vo, *Sci. Rep.*, 2021, **11**, 14787.
32 J. Wang, B. Gao, M. Dou, X. Huang and Z. Ma, *Environ. Res.*, 2020, **184**, 109339.
33 Y. Wang, Y. Tian, L. Yan and Z. Su, *J. Phys. Chem. C*, 2018, **122**, 7712–7719.
34 Y. Wen, D. Qu, L. An, X. Gao, W. Jiang, D. Wu, D. Yang and Z. Sun, *ACS Sustainable Chem. Eng.*, 2018, **7**, 2343–2349.
35 Y. Xiao, G. Tian, W. Li, Y. Xie, B. Jiang, C. Tian, D. Zhao and H. Fu, *J. Am. Chem. Soc.*, 2019, **141**, 2508–2515.
36 Y. Xing, X. Wang, S. Hao, X. Zhang, X. Wang, W. Ma, G. Zhao and X. Xu, *Chin. Chem. Lett.*, 2021, **32**, 13–20.
37 Y.-x. Zhang and Y.-h. Wang, *RSC Adv.*, 2017, **7**, 45129–45144.
38 H. Yu, R. Shi, Y. Zhao, T. Bian, Y. Zhao, C. Zhou, G. I. N. Waterhouse, L. Z. Wu, C. H. Tung and T. Zhang, *Adv. Mater.*, 2017, **29**, 1605148.
39 Y. Gong, X. Zhao, H. Zhang, B. Yang, K. Xiao, T. Guo, J. Zhang, H. Shao, Y. Wang and G. Yu, *Appl. Catal., B*, 2018, **233**, 35–45.
40 L. Jiang, X. Yuan, G. Zeng, J. Liang, Z. Wu, H. Yu, D. Mo, H. Wang, Z. Xiao and C. Zhou, *J. Colloid Interface Sci.*, 2019, **536**, 17–29.
41 J. Li, Y. Wang, X. Li, Q. Gao and S. Zhang, *J. Alloys Compd.*, 2021, **881**, 160551.
42 M. Zhang, Y. Li, W. Chang, W. Zhu, L. Zhang, R. Jin and Y. Xing, *Chin. J. Catal.*, 2022, **43**, 526–535.
43 D. Zhao, C. L. Dong, B. Wang, C. Chen, Y. C. Huang, Z. Diao, S. Li, L. Guo and S. Shen, *Adv. Mater.*, 2019, **31**, 1903545.
44 D. Zhu and Q. Zhou, *Appl. Catal., B*, 2021, **281**, 119474.